

Structural and Physical Properties Study of Some Iron Doped Mixed Manganite Perovskite SamplesA. G. Mostafa^{1*}, S. A. Mazen² and A. El-Attar²¹. Phys. Dept., Faculty of Science, Al Azhar Univ., Cairo, Egypt². Phys. Dept., Faculty of Science, Zagazig Univ., Zagazig, Egypt*drahmedgamal@yahoo.com

Abstract: Polycrystalline perovskite manganite samples of the composition $\text{La}_{0.7}\text{Ba}_{0.3}\text{Mn}_{1-x}\text{Fe}_x\text{O}_3$ ($0.0 \leq x \leq 0.5$), have been prepared by high energy ball-milling technique. The effect of replacing some manganese by iron cations on the structure of the studied samples, have been examined applying XRD. The obtained results indicated that, complete perovskite tetragonal structure has been obtained after milling the powder oxides for 36 hrs. The obtained crystallites were found mostly in the range of nano-particle size and the mean unit cell parameters were found approximately unchanged while the micro-strain showed slight increase. The calculated theoretical density showed very slight increase while both the apparent and relative densities showed an observable gradual increase. The magnetic susceptibility values showed gradual increase which may be due to the gradual increase of iron cations. The dc electrical transport measurements showed that all samples behave like semiconductors and the conduction mechanism was found to obey the variable range hopping (VRH) model. The electrical activation energy values were found to be connected tightly with the density of states at Fermi level.

[Mostafa AG, Mazen SA and El-Attar A. **Structural and Physical Properties Study of Some Iron Doped Mixed Manganite Perovskite Samples.** *Nat Sci* 2014;12(2):112-121]. (ISSN: 1545-0740). <http://www.sciencepub.net/nature>. 17

Keywords: High energy ball milling; Manganite perovskite; XRD analysis; Electrical transport; Magnetic susceptibility.

1. Introduction

During the last few decades, perovskite mixed manganite of the general composition $\text{R}_{1-x}\text{A}_x\text{MnO}_3$ (where R, represents a rare earth cation while A represents an alkaline earth or alkali cation), appeared to be of high importance due to their interesting electrical and magnetic properties. Therefore, they have very interesting applications in magnetic recording heads, magnetic sensorsetc [1, 2]. Their colossal magneto-resistance (CMR) phenomenon, metallic behavior and strong ferromagnetic interaction are generally based on the double exchange (DE) interaction model [3]. In this model there is an exchange of electrons between Mn^{3+} and Mn^{4+} cations through an oxygen anion when their core spins are parallel, since hopping is not favored when they are anti-parallel. Beside DE mechanism, Jahn–Teller character of Mn^{3+} cations show different aspects by introducing a variable electron–phonon coupling [4], and in particular two segregated phases with respectively, anti-ferromagnetic (AFM) and ferromagnetic (FM) ordering have been considered [5].

It is known that lanthanum manganite perovskite (LaMnO_3) has basically an anti-ferromagnetic insulator (AFI) behavior characterized by the super-exchange (SE) coupling between Mn^{3+} cations. By changing the oxygen stoichiometry or by substituting a divalent cation A^{2+} replacing La^{3+} , a percentage of Mn^{4+} cations appeared and LaMnO_3 can

be changed to metallic state, and hence, it exhibits a ferromagnetic ground state which was ascribed to DE.

More recently, some studies have been carried out in which doping was done also at the Mn-site. It has been suggested that introducing other transition metal element, which exhibit dissimilar electronic configuration to Mn-site should lead to dramatic effects associated with the electronic configuration mismatch between Mn and the other substituted magnetic cation. The nearest-neighbor compound of LaMnO_3 is iron oxide perovskite (LaFeO_3), and it is supposed that it has similar magnetic and transport properties, i.e. insulating and anti-ferromagnetic. However, it is supposed also that, the hole-doped $\text{La}_{1-x}\text{A}_x\text{FeO}_3$ perovskite have an anti-ferromagnetic ground state and remains insulating even at the maximum hole-doping extent [6].

The electrical transport in manganites is closely related to the spin of the e_g carriers and the localized t_{2g} spin core in Mn^{3+} cations, which is explained by the DE model and Jahn–Teller lattice distortion [7]. The 3d electrons of Mn^{4+} and Fe^{3+} cations are known to occupy the same spin state, due to strong Hund's coupling. The vacant state with opposite spins lies higher in energy due to the exchange interactions. Both occupied and unoccupied spin states are further split into t_{2g} and e_g orbitals by the octahedral crystal field. The replacement of Mn^{3+}

by Fe^{3+} dilutes the DE mechanism, suppresses the metallic conduction and enhances the insulating behavior. Hence, the mechanism that terminates the DE process arises purely from the electronic structure of these materials [8].

However, it is supposed that the substitution of Mn^{4+} by Fe^{3+} leads to an interesting modifications in their magnetic and electrical properties [9-11]. Therefore, this work will be carried out aiming to understand the relationship between the composition and the structural, magnetic and electrical properties of some polycrystalline manganite perovskite samples prepared by high energy ball milling, when some manganese will be replaced gradually by iron cations.

2. Experimental

Some perovskite manganite samples having the composition $[\text{La}_{0.7}\text{Ba}_{0.3}\text{Mn}_{1-x}\text{Fe}_x\text{O}_3]$ with $x = 0.0, 0.1, 0.2, 0.3, 0.4$ and 0.5] were prepared by using high energy ball milling technique (planetary mono mill, pulverisette (6) Fritsch GmbH). La_2O_3 , BaO , MnO and Fe_2O_3 , were used as raw materials, and their purity were not less than 99.5%. An electric balance with four decimal digits was used for weighting the powder oxides. Ethanol was added into the agate vial with the powders as a milling medium. The ratio of ball to powder weights was 10:1, and the rotating speed was set to be 500 rpm. After milling for 36 hrs, the mixture was dried in air to remove ethanol and then pressed into pellets. The pellets were calcinated at 1050 K for 5 hrs and the furnace was then raised and the samples were sintered at 1350 K for 24 hrs. The structure of the obtained samples was examined by X-ray diffraction (XRD), using Siemens D-500 powder diffractometer with CuK_α radiation ($\lambda = 0.154$ nm). Archimedes technique was applied to measure the apparent density (AD) of the studied samples. The theoretical density (TD) as well as the relative density (RD) was also calculated. Gouy method was used to measure the magnetic susceptibility of the studied samples with an electromagnet of 5 T max. The dc electrical measurements were carried out in the temperature range from 300 up to 450 K using VA-J-52 electrometer.

3. Results and Discussion

3.1. X-Ray Diffraction (XRD)

The structural characterization of the studied samples was carried out by using XRD at room temperature and under the ambient conditions. Fig (1) shows the obtained XRD patterns of the samples no. 1, 3 and 6 (those containing 0.0, 0.2 and 0.5 Fe) as representative patterns, after refining applying the

Rietfitted analysis under the Fullprof program. These patterns indicated that a single manganite perovskite crystalline phase was prepared. The major phase has a tetragonal structure with main unit cell parameters of $a = b = 3.921 \text{ \AA}$ and $c = 13.175 \text{ \AA}$, with space group 14/mmm [12].

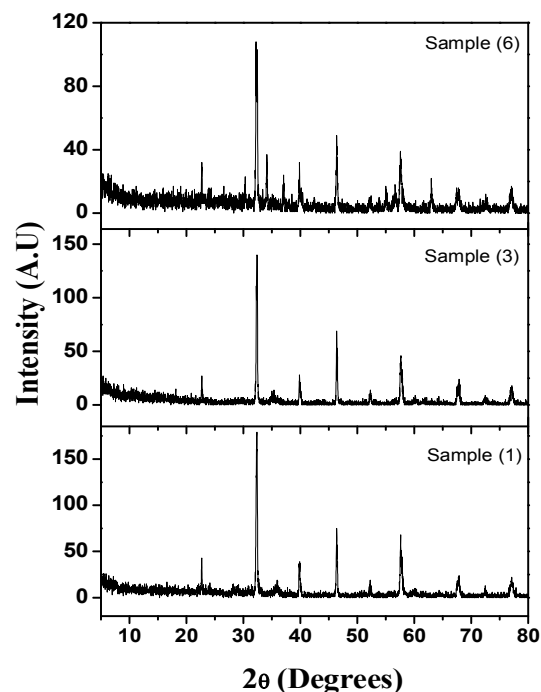


Figure 1. XRD patterns for samples no. 1, 3 and 6, as representative patterns.

It is worth to state that, a single phase perovskite samples could not be obtained except after milling the powder oxides for 36 hrs and carrying out the calcination and sintering of the pressed pellets for 5 hrs at 1050 K and for 24 hrs at 1350 K respectively. This long milling and sintering times may be due to the substitution in both A and B sites (that is, the replacement of some La^{3+} by Ba^{3+} and some Mn^{4+} by Fe^{3+} cations).

The observed sharpness of the XRD peaks indicated that the samples are fully crystallized. In order to distinguish the effect of crystallite size and strain induced broadening at full width at half maximum (FWHM) of the XRD profiles, Williamson–Hall (W-H) plots were performed, and Fig (2) shows such plot for the sample no.(3), as representative curve (W-H plot is the integral breadth in the reciprocal space ($\Delta K = \beta \cos \theta / \lambda$, β -FWHM of XRD line) with respect to reciprocal lattice space ($K = 2 \sin \theta / \lambda$)) [13]. The average particle size (D) of the

obtained nano-crystallites was calculated by using (W-H) method, according to equation no. (1) (Williamson–Hall eq),

$$\beta \cos(\theta) = \frac{c\lambda}{D} + 4\varepsilon \sin(\theta) \quad (1)$$

Where (c) is the correction factor ($c \approx 0.9$), ($\lambda = 0.154$ nm) is the wave length of the CuK_α radiation, (θ) is the Bragg angle at the X-ray diffraction peak, (β) represents the corrected full width at half

maximum of the diffraction peak in radians and (ε) is the micro-strain.

The calculated values of both the particle size and strain are exhibited in Table (1), where it is seen that, as manganese was gradually replaced by iron cations, the particle size shows noticeable gradual increase while the micro-strain shows very slight increase. Such increase can be attributed to the size difference between iron and manganese cations that makes some distortion in the structure of the prepared perovskite samples. It is supposed also that, iron cations may act to agglomerate the formed perovskite particles [14].

Table 1. The obtained particle size (D) and strain (ε), versus iron content.

X(Fe)	0	0.1	0.2	0.3	0.4	0.5
Particle size (D) (nm)	53	67	86	99	106	115
Strain (ε)	0.00082	0.00097	0.00128	0.00142	0.00155	0.00164

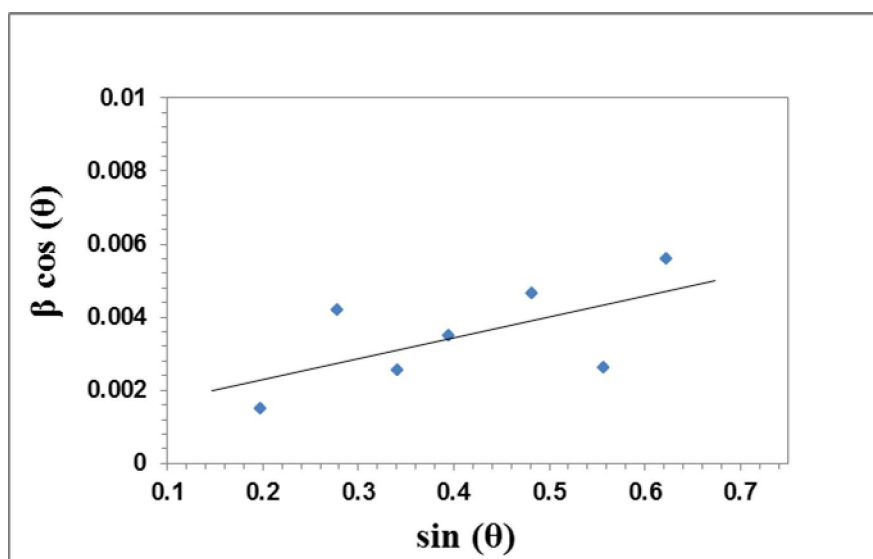


Figure 2. W- H plot for sample no. (3), as representative curve.

3.2. Density Measurements

Density of a material is a property of importance, since it reflects directly the fine changes in the structure, phase transformation, structural rearrangement etc., that can be attributed to any differences in composition, thermal history or milling time during preparation. That is, any observed changes in the density have to evidence some logic changes in the structure and hence some changes in the internal free volume.

It is of interest also to compare the apparent density (AD) values with those obtained theoretically. However, the theoretical density (TD) values were also calculated by using the unit cell data that obtained from XRD patterns applying the following equation (no. 2) [15],

$$\rho_{th} = \frac{[n(\sum A_C + \sum A_A)]}{V_c * N_A} \quad (2)$$

where, n is the number of formula units, (that is all ions included in the unit chemical formula within the unit cell), $\sum A_c$ is the sum of the atomic weights of all cations in the formula unit, $\sum A_A$ is the sum of the atomic weights of all anions in the formula unit, V_c is the unit cell volume calculated from X-ray data and N_A is Avogadro's number (6.023×10^{23} per mole).

Accordingly, the experimentally obtained AD values of the studied perovskite samples and those obtained theoretically (using XRD data) as well as the relative density ($RD = AD / TD$) were all exhibited in Table (2).

It can be seen, from this table, that all the measured and the calculated density values increased gradually but with different rate of change. Both the AD and the TD are represented graphically in Fig. (3) (for comparison) as a function of iron cations content, where an obvious gradual linear increase can be easily observed for the measured AD, while non-observable increase in the TD appears. The rate of change in the AD was calculated to be = $1.93 \text{ (g. cm}^{-3})$

$\cdot \text{mol}^{-1}$), while that of the TD was found to be = $0.038 \text{ (g. cm}^{-3} \cdot \text{mol}^{-1})$.

The non-observable change (very low rate of change) of the TD may be due to the similarity between iron and manganese cations, where they are nearest neighbors in the periodic table. On the other hand, the observable change (high rate of change) in the AD can be attributed to the gradual rearrangement in the structure of the prepared perovskite samples. That is when iron cations entered the lattice replacing manganese; they may arrange themselves in a manner which decreases the internal free volume, with some increase in the mean molecular weight of the sample. This may logically increase the AD gradually, that is, iron cations act to decrease the pores in the lattice [15]. This result was found in agreement with that obtained from XRD, that is, iron act to agglomerate the formed perovskite particles and hence increase slightly the particle size [14].

Table 2. Theoretical, apparent and relative densities of the studied samples versus iron content.

X(Fe)	0	0.1	0.2	0.3	0.4	0.5
TD	9.892	9.896	9.899	9.904	9.907	9.911
AD	8.489	8.666	8.934	9.104	9.368	9.454
RD	85.82%	87.57%	90.24%	91.93%	94.55%	95.39%

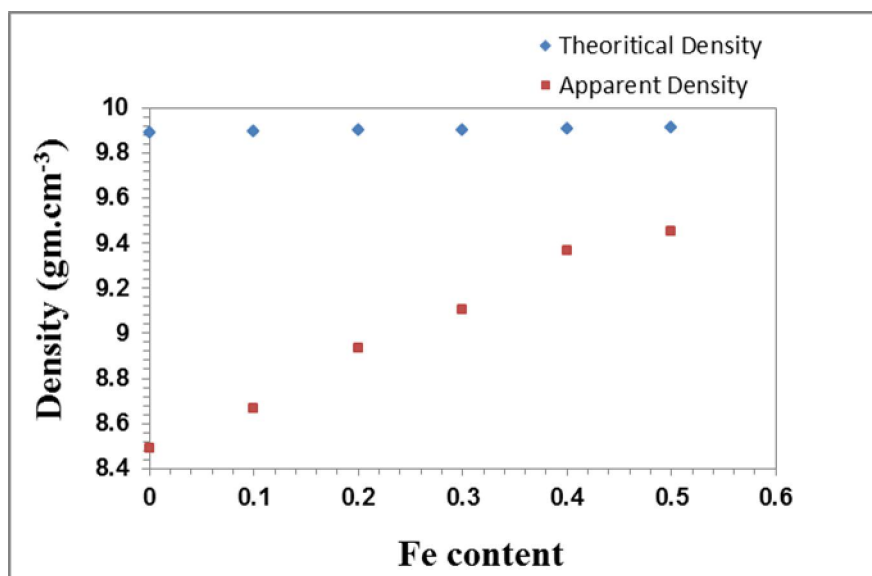


Figure 3. TD and AD of the studied perovskite samples versus iron.

3.3. Magnetic Susceptibility

It is well known that the magnetic behavior of manganite perovskite materials is a matter of interest due to their various applications. The appearance of magnetism in manganites with perovskite structure is due mainly to the interplay between the super-exchange and double exchange interactions and their magnetic behavior depend usually on the following factors [16]:

- (1) The amount of iron content in a perovskite sample.
- (2) The percentage of the divalent cations.
- (3) The average ionic radii of the metal cations.
- (4) The method of preparation.

However, applying Gouy method, the differences in the weights of a sample (dm) due to the change in the intensity of the applied magnetic field (H) were recorded, and were then plotted in Fig. (4) as a function of H^2 . The slopes (dm/dH^2) for the studied samples were obtained and the volume magnetic susceptibilities (K) were then calculated [17] employing equation (3),

$$K = \left(\frac{2g}{a} \right) \cdot \left(\frac{dm}{dH^2} \right) \quad (3)$$

Where g is the acceleration due to gravity and a is the cross sectional area of the measured sample.

The mass magnetic susceptibility values (M) were then calculated applying equation (4),

$$M = \frac{K}{d} \quad (4)$$

where d is the measured apparent density.

Multiplying the mass magnetic susceptibility by the mean molecular weight of each sample (W), the molar magnetic susceptibility (ϕ) was then obtained using equation (5),

$$\phi = M * W \quad (5)$$

The calculated values of the volume, mass and molar magnetic susceptibilities are listed in Table (3).

The change in the molar magnetic susceptibility was also plotted in Fig. (5), as a function of iron content. Inspecting the obtained results presented in Table (3) and Fig. (5), it is easy to observe that, the obtained susceptibility values increased gradually as iron cations were gradually increased. This behavior seems to be logic, where iron cations exhibit high ferromagnetic character, since Fe^{3+} cations have five parallel spin electrons, aligned with the applied field and hence enhance the magnetization of the studied samples gradually.

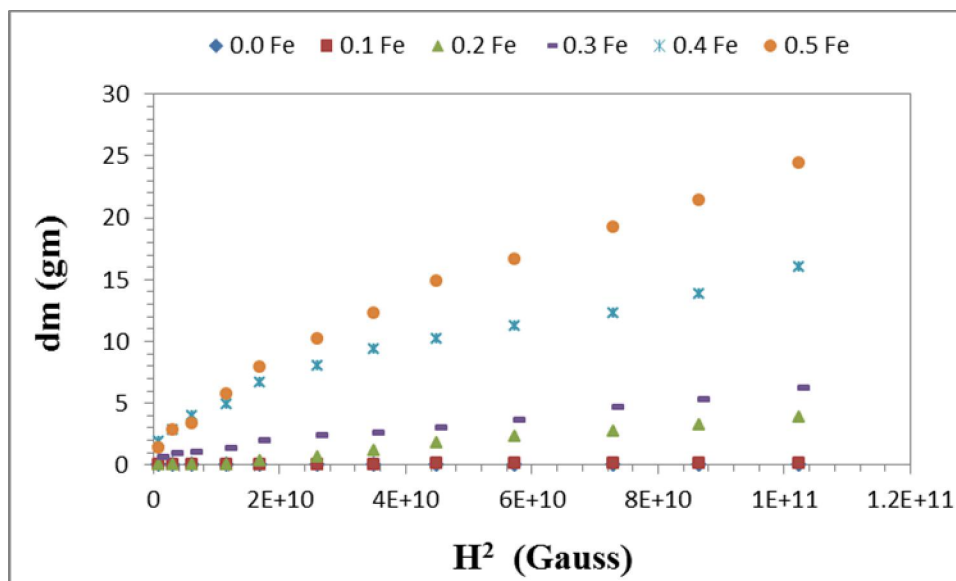


Figure 4. The change in dm as a function of H^2 .

Table 3. The magnetic susceptibilities; (K in $\text{esu} \cdot 10^{-7}$, M in $\text{esu} \cdot \text{cm}^{-3} \cdot \text{gm} \cdot 10^{-8}$ and ϕ in $\text{esu} \cdot \text{cm}^{-3} \cdot \text{mol}^{-1} \cdot 10^{-5}$).

X(Fe)	0	0.1	0.2	0.3	0.4	0.5
K	0.084	1.014	24.981	32.959	77.370	135.000
M	0.099	1.170	27.963	33.280	82.594	142.280
ϕ	0.036	0.431	10.501	12.740	32.220	56.743

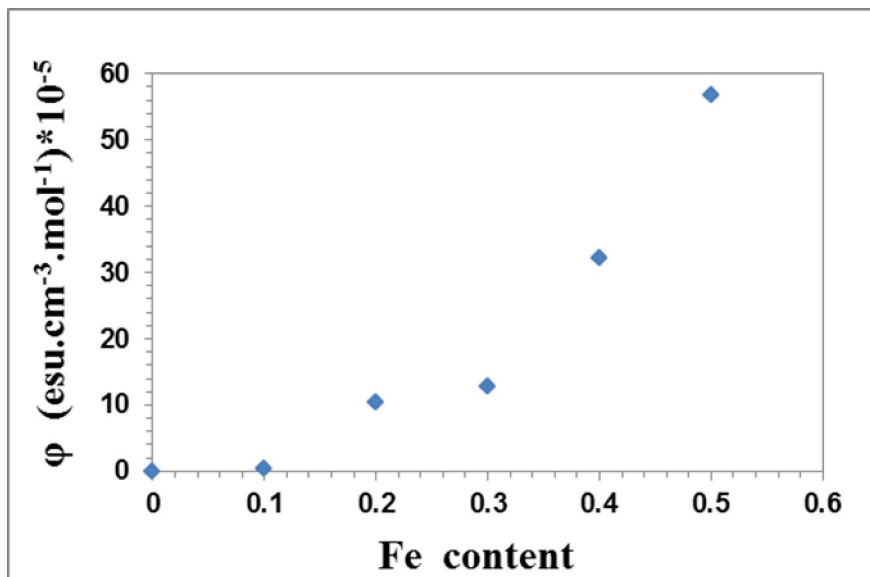


Figure 5. The change in the molar magnetic susceptibility versus iron content.

3.4. DC Electrical Conductivity

The dc electrical conductivity was measured in the temperature range from 300 and up to 450 K, and Fig. ((6) a, b) shows the relation between ($\ln \sigma$) versus the reciprocal of temperature ($1/T$) for the samples containing 0.0 and 0.5 iron (as representative curves), where straight lines were clearly observed for both samples, and it is worth to state that, all samples show similar behavior.

The activation energy (ΔE) values were also calculated applying Arrhenius equation (equation no. 6) and were exhibited in Table (4) as a function of iron content.

$$\sigma_T = \sigma_o \exp\left(\frac{\Delta E}{k_B T}\right) \quad (6)$$

Where:

σ_o : is the pre-exponential factor.

ΔE : is the activation energy.

T : is the absolute temperature.

k_B : is Boltzmann constant.

From Table (4), it can be seen that ΔE decreases from 0.21 to 0.12 eV, as the iron content was increased from 0,0 to 0.2, then it starts to increase again up to 0.21 eV corresponding to an iron content value of 0.5. For the first sight, this result seems to be non-logic, and in order to examine such behavior, the conduction mechanism in these samples must be identified. Then, the number of cations per unit volume, the inter-ionic distance and the density of states at Fermi level, all these factors must be investigated.

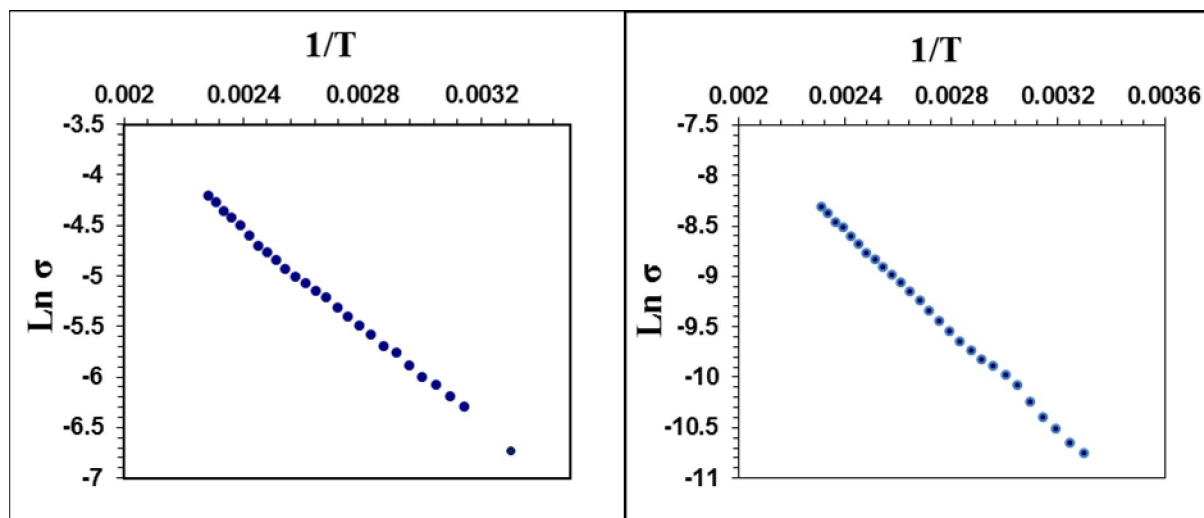


Figure 6. a, b, Plots of $(\text{Ln } \sigma \text{ s.m}^{-1})$ versus $(1/T \text{ K}^{-1})$ for the samples containing 0.0 and 0.5 iron respectively, as representative curves.

Table 4. The change in the activation energies (ΔE) versus iron content.

X(Fe)	0	0.1	0.2	0.3	0.4	0.5
ΔE (eV)	0.21	0.16	0.12	0.15	0.19	0.21

In order to conclude the conduction mechanism, three models have to be checked. These models are the thermally activated behavior (Arrhenius), the small polaron hopping (SPH) and the variable range hopping (VRH) [18-20]. They can be evaluated by calculating the linear correlation coefficient (R^2), which can be obtained by fitting the experimentally obtained conductivity values with the theoretical equations for all these models. Fig. ((7) a, b) exhibits representative curves for the fitting of the obtained data due to samples number (1) and (6) (those containing 0.0 and 0.5 iron cations respectively), applying the theoretical equation of VRH model [equation (7)]. It is appeared that all the studied samples fit well as straight lines, and it is worth to state that all samples show similar behavior. The linear correlation coefficient (R^2) was found between 0.998 and 0.999 for all samples. It was expected also that, electrons represent the main charge carrier in all the studied samples.

$$\sigma(T) = \sigma_0 \exp \left[- \left(\frac{T_0}{T} \right)^{1/4} \right] \quad (7)$$

Applying this model, the concentration of cations per unit volume, the inter-ionic distances between these cations and the density of states at Fermi level, can be obtained. The number of cations per unit volume ($N \text{ cm}^{-3}$) [21] was calculated using the following equation, (no. (8)),

$$N = \frac{\rho N_A}{M} \quad (8)$$

Where:

ρ : is the AD of a sample.

N_A : is Avogadro's number.

M : is the mean molecular weight of such sample.

The relationship between (N) and the mean inter-ionic distance (L) [22, 23] is generally described by equation no. (9),

$$L = \left(\frac{1}{N} \right)^{1/3} \quad (9)$$

The density of states at Fermi level can be also calculated from equation no. (10) [24],

$$N(E_F) = \frac{3}{4\pi R^3 \Delta E} \quad (10)$$

Where, ΔE represents the activation energy of the sample under investigation. All the obtained results are illustrated in Table (5).

Also, Fig. (8) exhibits the change in the density of states at Fermi level as well as the activation energy as a function of iron content.

From both, Table (5) and Fig. (8), it can be stated that both the number of ions (N) and the inter-ionic distances (L) appeared to be approximately unchanged (fluctuated approximately around a stable value for each), while the density of states at Fermi

level shows gradual increase until iron content reaches 0.2, then it starts to decrease gradually again. According to the obtained values of both ΔE and $\ln \sigma$, it can be stated that, all samples behave like semiconductors [25]. In the range of measurements, the activation energy (ΔE) was found to depend on the density of states at Fermi level, where the first decrease in ΔE may be due to the observed increase in the density of states, but the latter increase of ΔE can be attributed to the gradual decrease of the calculated density of states. On the other hand, as Fe^{3+} content was gradually increased, the number of cations per unit volume as well as the inter-ionic distance seems to be fluctuated around stable values, and therefore they have no effect on ΔE .

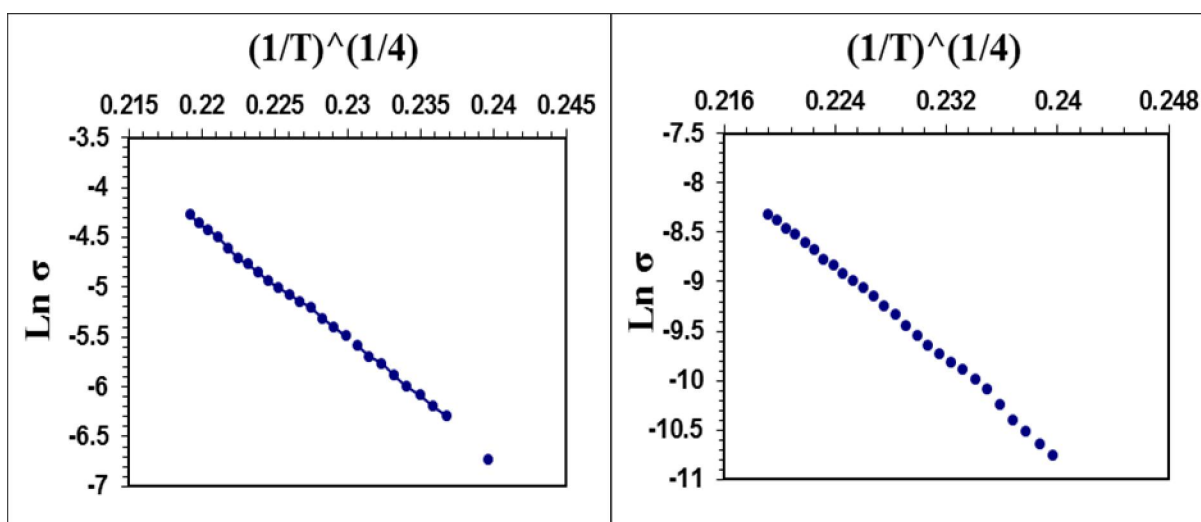


Figure 7. a, b, The fitting of the experimental data (solid points) for the samples containing 0.0 and 0.5 Fe cations respectively with the theoretical equation of the VRH model (solid line), which is the best one to describe the conduction mechanism.

Table 5. Number of ions (N), inter-ionic distance (L) and density of states $N(E_F)$ at Fermi level.

X(Fe)	0	0.1	0.2	0.3	0.4	0.5
$N \text{ cm}^{-3} \times 10^{22}$	1.4164	1.4173	1.4327	1.4324	1.4463	1.4330
L nm	0.4133	0.4132	0.4117	0.4118	0.4104	0.4117
$N(E_F)(\text{ev})^1 \cdot \text{cm}^{-3} \times 10^{22}$	1.6254	2.1578	2.7425	2.2775	1.8525	1.6192

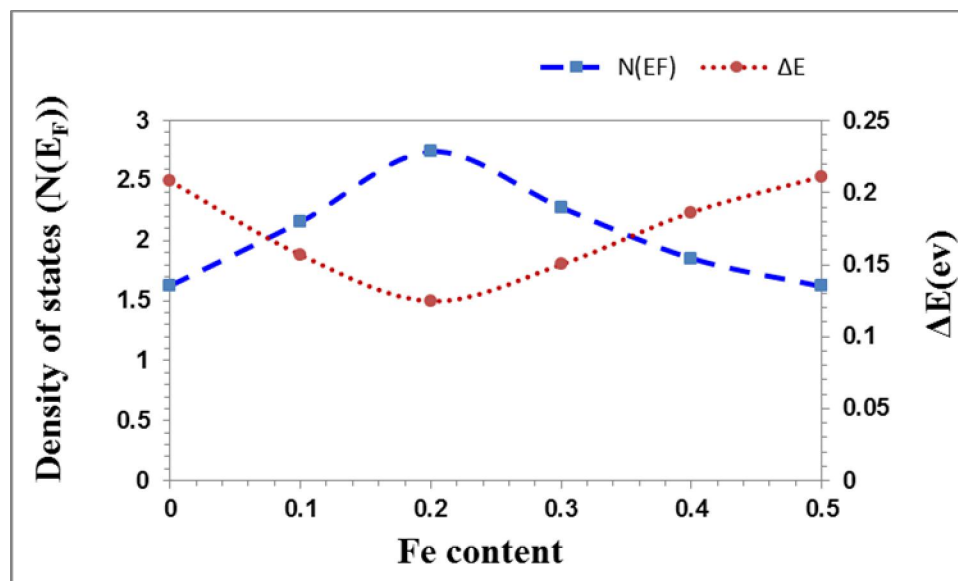


Figure 8. The change in the density of states and the activation energy versus iron content.

4. Conclusion

According to the above studies, it can be concluded that, the replacement of some Mn by Fe cations in the studied perovskite samples set slight distortion in the lattice, which could not be detected by XRD analysis. That is, the lattice parameters appeared to be approximately unchanged, but the particle size and micro-strain showed gradual increase with the gradual increase of iron cations. The apparent density increased which may be due to the effect of iron to agglomerate the formed perovskite particles and to decrease the pores. It was found that, the magnetic susceptibility values directly affected, to a large extent, by Fe doping which may be due the dissimilarity of the electronic spins between manganese and iron as well as the higher ferromagnetic character of iron. It was found also that, all the studied perovskite samples behave like semiconductors and the variable range hopping (VRH) model is the applicable conduction mechanism. It can be concluded also that ΔE values are logically connected to the density of states at Fermi level, while the number of cations per unit volume and the inter-cationic distances are of no effect.

Corresponding Author:

Prof. Dr. Ahmed G. Mostafa
Physics Department.
Faculty of Science
Al Azhar University, Cairo, Egypt
E-mail: drahmedgamal@yahoo.com

References

1. S. Jin, M. Mc Cormack, T. H. Tiefel and R. Ramesh, *J. Appl. Phys.*, 76 (1994) 6929.
2. J. Yang, Y. Q. Ma, R.L. Zhang, B. C. Zhao, R. Ang, W. H. Song and Y. P. Sun, *Solid State Commun.*, 136 (2005) 268.
3. C. Zener, *Phys. Rev.*, 82 (1951) 403.
4. A. J. Millis, P. B. Littlewood and B. I. Shraiman, *Phys. Rev. Lett.*, 74 (1995) 5144.
5. E. Dagotto, T. Hotta and A. Moreo, *Phys. Rep.*, 344 (2001) 1.
6. T. Peterlin-Neumaier and E. Steichele, *J. Magn. Magn.Mater.*, 59 (1986) 351.
7. N. F. Mott, "Metal-Insulator Transitions", Taylor&Fracis, London, (1990).
8. K. H. Ahn, X.W. Wu, K. Liu and C.L. Chien, *Phys. Rev. B*, 54 (1996) 15299.
9. S. Jin, T. H. Tiefel, M. Mecormack, R. A. Fastnacht, R. Ramesh and L. H. Chen, *Science*, 264(1994) 413.
10. A. Ajana, N.Venkataramani, S. Prasad, S. N. Shringi, A. K. Nigam and R. Pinto, *J. Appl.Phys.*, 83 (1998) 7169.
11. Darshan C. Kundaliya, R. Vija, R. G. Kulkarnia, A. A. Tulapurkarb, R. Pinto, S. K. Malikb and W. B. Yelon, *J. Magn. Magn.Mater.*, 264 (2003) 62.
12. M. Vallino, F. Abbattista, D. Mazza, *Mater.Res. Bull.*, 21 (1986) 733.
13. L. M. Su, N. Grote, F. Schmitt, *Electron lett.*, 20 (1984) 717.
14. D. P. Joseph, T. P. David, S. P. Raja and C. Venkateswaran, *Materials Characterization*, 59 (2008) 1137.

15. William D. Callister Jr, "Materials science and Engineering: An introduction", John Wiley and Sons Inc., 6th edition, New York, (2003).
16. S. L. Younga, H. Z. Chena, M. C. Koa, L. Horngb and Y.T. Shihb, *J. Magn. Magn. Mater.*, 303 (2006) 351.
17. Ahmed Gamal El-Din Mostafa, *Turk. J. Phys.*, 26 (2002) 441.
18. A. Banerjee, S. Pal and B. K. Chaudhuri, *J. Chem. Phys.*, 115 (2001) 1550.
19. G. J. Snyder, R. Hiskes, S. Dicarolis, M. R. Beasley and T. H. Geballe, *Phys. Rev. B*, 53 (1996) 14434.
20. D. Saritha, Y. Markandeya, M. Salagram, M. Vithal, A. K. Singh and G. Bhikshamaiah, *J. Non-Cryst. Solids*, 354 (2008) 5573.
21. M. S. Al-Assiri, M. M. El-Desoky, A. Al-Hajry, A. Al-Shahrani, A. M. Al-Mogeeth and A. A. Bahgat, *Physica B*, 404 (2009) 1437.
22. M. M. El-Desoky, *Mater. Chem. Phys.*, 119 (2010) 389.
23. A. A. Bahgat, B. A. A. Makram, E. E. Shaisha, M. M. El-Desoky, *J. Alloys and Compounds*, 506 (2010) 141.
24. D. Emin and T. Holstein, *Ann. Phys.*, 53 (1969) 439.
25. L. Pi, L. Zhang and Y. Zhang, *Phys. Rev. B*, 61 (2000) 8917.

1/29/2014